PROCEEDINGS, 48th Workshop on Geothermal Reservoir Engineering
Stanford University, Stanford, California, February 6-8, 2023
SGP-TR-224

Preliminary Hydrogeologic Characterization of the Cornell University Borehole Observatory (CUBO), Ithaca NY

Roberto D. Clairmont[1], Patrick M. Fulton[1], Teresa E. Jordan[1]

[1]Department of Earth and Atmospheric Sciences, Cornell University, Ithaca, NY

rdc229@cornell.edu

Keywords: hydraulic diffusivity, permeability, modelling, pressure diffusion, Cornell University, deep direct-use, dual-packer, hydrogeologic air-lift test, reservoir.

1 ABSTRACT

The Cornell University Borehole Observatory is a 9790 ft deep well drilled into Pre-Cambrian basement for the purpose of identifying the feasibility of deep direct-use district heating (DDU) of the Cornell Campus via a DDU geothermal system. This follows Cornell's objective to obtain a carbon neutral campus by the year 2035. To incorporate such a system, target reservoir formations at depth should provide adequate temperature and fracture permeability for injection and production at a flow rate that will maintain a suitable lifetime of the reservoir. One of the primary objectives is to understand the hydrological properties of target formations. Here we present data and initial findings obtained from several tests that provide insights into the subsurface hydrogeologic characteristics.

Following completion of drilling in mid-August 2022, several days of logging and testing were conducted within the open section of the borehole (7656 - 9790 ft). Acoustic and resistivity image logs from borehole imaging (BHI) indicate the presence of fractures, identifying regions of interest where sufficient fracture permeability may exist. Near the end of operations, production and injection tests were conducted in the full borehole. First an airlift test was conducted that progressively lowered the borehole water level to ~4000' below ground surface. Based on observations of water level and P-T logs run during and after the test, the borehole did not appear to produce significant flow. Reinjection of the displaced water and pressurization with mudpumps up to 1400 psig, also did not appear to drive considerable flow into the formation.

These data suggest the formations spanning the Ordovician-Pre-Cambrian strata are relatively low permeability. However, there are indications of localized fracture permeability and connectivity based on correlative signatures from several other logs and tests. For instance, online gas analysis by mass spectrometer during drilling reveals numerous intervals with inflows of inorganic gases, particularly Hydrogen and Helium. The depth interval with the highest fluxes corresponds with fracture networks identified within dolomitized sandstone units within the Galway Formation between depths 8670 – 8710 ft depth. Dual packer experiments, primarily used for minifrac tests and stress analysis targeted fractures identified at 8685 and 8695 ft and show evidence of fracture permeability – at least when borehole fluid pressures are relatively high. Analyzing the diffusion of pressure during these experiments provides constraints on hydraulic diffusivity within one of the target intervals under investigation for potential development as an EGS reservoir.

2 INTRODUCTION AND MOTIVATION

Fluid flow and pressure diffusion within the subsurface is controlled by hydrogeologic properties. Characterizing these properties is important for understanding the location, direction, and effectiveness of potential flow paths for heat exchange within a geothermal well system and guide subsequent well design. In addition, where permeability is insufficient for substantial flow, hydrogeologic characterization can help guide effective stimulation programs. Identification and hydrogeologic characterization of potential geothermal reservoir intervals is therefore a major objective of the Cornell University Borehole Observatory (CUBO). CUBO is a 9790.5 ft deep geothermal exploratory well drilled in 2022 on Cornell University's Ithaca, New York campus in order to explore the potential for developing a deep direct-use geothermal system for district heating, which Cornell refers to as Earth Source Heat (ESH) (Beckers et al. 2021; Gustafson et al. 2020; Jordan et al. 2020; Tester et al.2019 and Tester et al. 2020) (see also the companion paper by Tester et al., 2023).

Two of the biggest technical uncertainties with geothermal projects in hard, fracture-dominated systems like in upstate New York concern: 1) uncertainty as to the interconnectivity of natural fracture pathways accommodating fluid flow for establishing injecting and producing well pairs and 2) uncertainty in the hydrogeologic properties of the rock body. Here, we describe a series of logging and testing data collected during CUBO drilling, along with an integration of other observations and characterizations presented in companion papers (Fulcher et al., 2023; Purwamaska and Fulton, 2023) that together provide a broad quantitative and qualitative understanding of the subsurface hydrogeology. The bulk of the analysis presented here is based on analysis of pressure buildup data during dual-packer hydraulic testing experiments that provide estimates of the background hydraulic diffusivity. These data along with the overall characterization of the hydrogeology and permeability architecture within the subsurface provide important constraints on modeling and subsequent well and stimulation design. The integration of hydrogeologic information from various datasets highlights the relatively low transmissivity of the well while also highlighting several permeable zones of particular interest as potential reservoir targets.

3 METHODS

After completion of drilling, a suite of logging and testing was completed within what remains as an open-hole section within CUBO from 7656 - 9790 ft to identify and characterize target zones for reservoir potential. Data from several sets of wireline logging consist of petrophysical and sonic wireline logs and borehole imaging. In addition, hydraulic experiments using a dual-packer system were conducted at four different depth intervals, primarily for determining stress magnitude (see companion paper Pinilla et al., 2023). Subsequently, the hole was wiped clean again and a series of hydrologic tests combined with high-resolution temperature logs were performed. These tests consisted of an airlift test that lowered the hydraulic head within the well to try to induce flow into the well followed by an injection test in which water was returned to the well and a modest back pressure was applied in attempt to drive fluid flow into the formation. The following describes several types of datasets and methodologies used to garner insights into hydrogeologic characteristics of the subsurface.

3.1 Wireline Logging

Wireline logging tools measure the mechanical, physical, chemical, and electrical properties of the rock along the borehole. The measured logs are presented as an array of continuous recording of a geophysical parameter per 0.5 - 1ft. A Triple Combo logging tool was used to measure total and spectral gamma ray, caliper width, porosity, acoustic velocities, and electrical resistivity logs. Logs used to identify hydrological properties especially porosity include, neutron porosity (NPHI), density porosity (DPHI) and sonic porosity (SPHI). A commonly utilized log combination is the use of the neutron-density porosity logs as a gas detection method. The presence of gas within the pore space can increase the density porosity and reduce the neutron porosity (lower concentration of hydrogen atoms in gas compared to oil or water) observed as a gas effect/neutron-density crossover along the logs (Asquith & Krygowski, 2004). For the analysis in this paper, we use the gas effect/crossover of the neutron and density porosity logs in addition to the sonic porosity log to identify zones of potential permeability.

3.2 Gas Chromatography Analysis

Gas analysis via a wellsite mass spectrometer was conducted during drilling to measure the quantity of specific organic and inorganic compounds present within the drilling mud circulating out of the hole. Measurements include total gas; C_1-C_5 hydrocarbon concentrations; inorganic helium, hydrogen, and carbon dioxide concentrations; and atmospheric concentrations of argon, oxygen, and nitrogen. Analysis of drilling mud gas utilized an inline constant volume degasser connected to a DQ1000 mass spectrometer. A 1.5 L/min mud flow rate constantly entered the gas trap where the exhaust product was conveyed to and analyzed by the DQ1000. For the purposes of analysis here, Helium and hydrogen concentrations are used identify potentially permeable zones as indicators of connected permeability that extends sufficiently away from the borehole.

3.3 Fracture Distribution

Acoustic and resistivity borehole imaging (BHI) logs were used to obtain qualitative and quantitative information on fracture presence along the open section of the borehole. Imaging along the borehole included the utilization of an acoustic televiewer and three micro-resistivity surveys. Fracture frequency was calculated in 10-meter bins using processed borehole imaging analysis software (see companion paper by Fulcher et al., 2023 for full fracture interpretation and analyses).

3.4 Hydrologic Airlift Test

The objectives of the airlift test are, to determine characteristics of produced and injected water, which include flow rate and flowing temperature, and determine pressure loss as a proxy for drawdown during airlift and recovery after flow is stopped. During an airlift test, fresh water is placed into the well and air is injected through a coiled flow line or drill pipe run into the well to a certain depth below static water level. The static water level is achieved during a shut-in period. Compressed air injected through the flow line inadvertently causes the water column within the annulus to become aerated with bubbles. The density of fluid at the water-air column decreases and results in the aerated fluid level to rise back toward the surface. A PT-spinner (Pressure-Temperature) logging tool can be run during the test to identify regions of flow from subsurface formations along the borehole.

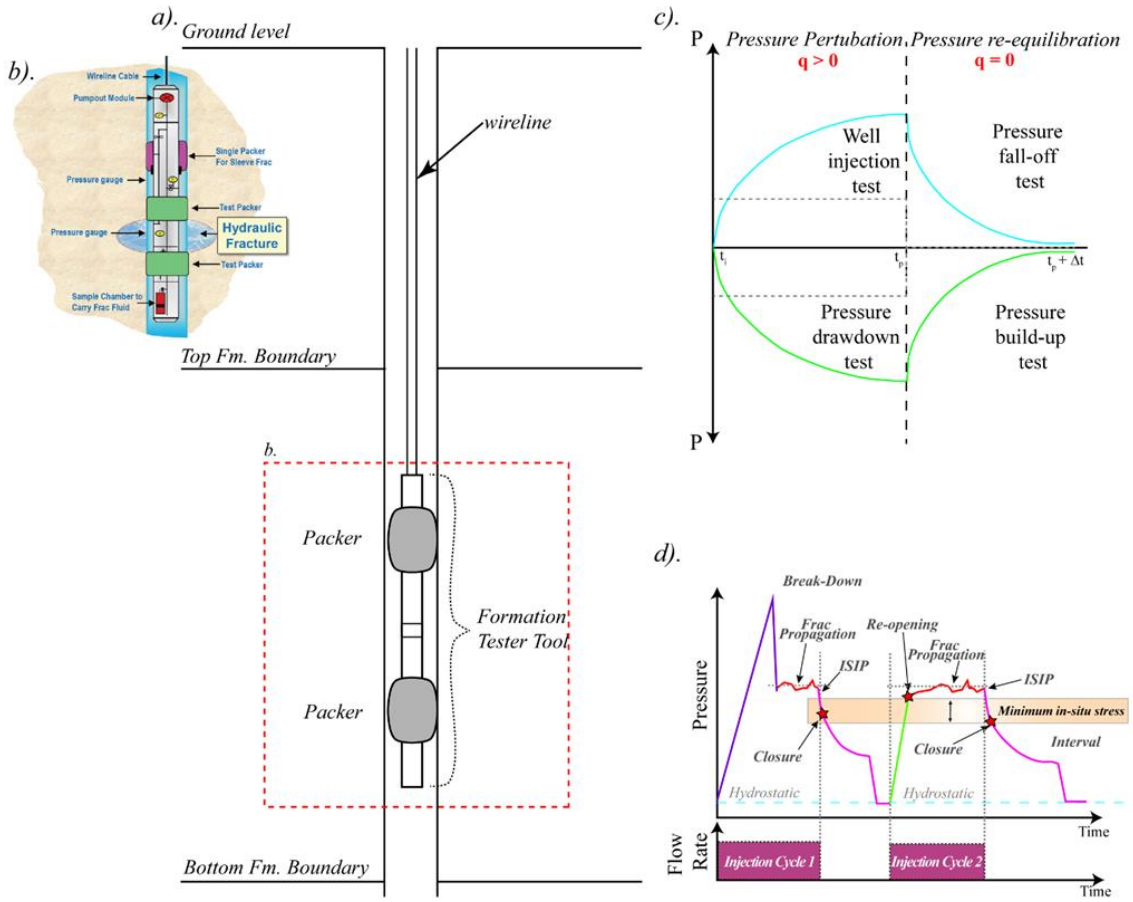

Figure 1. (a) Schematic of a dual-packer configuration in which two inflatable packers isolate a target interval from the rest of the borehole. (b) Detailed schematic of the dual-packer configuration with different components for deploying the taken from Malik et al. 2016. (c) Schematic of the behavior of pressure during varying types of well tests. (d) A conceptual but ideal illustration of the pressure response of a mini-frac test showing the breakdown pressure (fracture initiation), fracture propagation and closure for two injection cycles after Malik et al. 2016

3.5 Dual-Packer Experiment

Prior to the hydraulic tests described above, a series of dual-packer experiments were conducted at five depth intervals within the open-hole section. These tests were primarily for the purpose of determining stress magnitude (see companion paper Pinilla et al., 2023). Here, we utilize the pressure response data during these tests as a means to estimate the background hydraulic diffusivity of the formation within zones that are largely unfractured prior to testing. Figure 1 illustrates the general type of dual-packer hydraulic set-up and experiment conducted at CUBO.

The dual-packer test set up utilizes two inflatable packers that isolate a target interval from the rest of the borehole as shown in the schematic of Figure 1a and b. Fluid is injected into the isolated interval to build enough pressure to create a microfracture. Fluctuations in pressure signals are observed throughout the history of the test when perturbing the system isolated by the dual packers. A simple build up and recovery of pressure during such test is shown in Figure 1c. During an injection test, perturbation of the system results in a pressure build-up which rolls-over until the end of perturbation before decreasing during recovery or re-equilibration. The lower half of the schematic reflects the response of a pressure drawdown test – which was not conducted in this study. A more detailed and expected pressure response of a dual-packer experiment is shown in Figure 1d (after Malik et al., 2016). Different signals of the full history of the test provide specific information on in-situ pressure conditions. To interpret the pressure response through time, pressure transient techniques can be applied. Such techniques can be used to model and interpret the curves associated with pressure buildup, drawdown, fall-off and injection (Figure 1c.) to obtain reservoir properties (Earlougher, 1977; Matthews & Russell, 1967).

The pressure data reflects how the isolated formation interval, and dual-packer system, respond to fluid injection and can provide insights into the in situ hydraulic diffusivity around the borehole. Assuming well sealed packers, pressure buildup during injection is largely controlled by the water and system compressibility and by amount of fluid lost from the system due to pressure diffusion, i.e.,

fluid flow, into the formation. Here we analyze the pressure data during these experiments to estimate hydraulic diffusivity of the formation within the packered intervals.

We analyze the pressure response data utilizing an analytical solution for 1D diffusion that considers both the pressure build-up and subsequent recovery for a fluid source lasting a period of time t and where t^* represents the end of the perturbation period of the system prior to re-equilibration:

$$P(x,t)=\frac{Q}{\beta\rho}t\left(\left[1-2i^2\mathrm{erfc}\left(\frac{a-x}{(4Dt)^{\frac{1}{2}}}\right)-2i^2\mathrm{erfc}\left(\frac{a+x}{(4Dt)^{\frac{1}{2}}}\right)\right]-H(t-t^*)(t-t^*)\left[1-2i^2\mathrm{erfc}\left(\frac{a-x}{(4D(t-t^*)^{\frac{1}{2}}}\right)-2i^2\mathrm{erfc}\left(\frac{a+x}{(4D(t-t^*)^{\frac{1}{2}}}\right)\right]\right) \quad (1)$$

where P is pressure (Pa), Q = mass flow rate per volume (kg/m^3s) during perturbation (fluid injection), β is the compressibility (Pa^{-1}), ρ is the density (kg/m^3) of the fluid, H is the Heaviside function which is equal to 1 when the argument is 1 and 0 otherwise, *x* is the distance between the center of the borehole (m) and the borehole wall and *a* is the distance from the center of the borehole beyond the wall of the formation (m). The $i^2\mathrm{erfc}(\xi)$ terms represent the second integral of the complementary error function evaluated from ξ to infinity (Carslaw and Jaeger,1959). This novel approach for analyzing the dual packer pressure data follows a similar framework and solution developed for heat transfer (Lachenbruch, 1986; Fulton and Harris, 2012).

Following Eqn. 1, Figure 2 illustrates how pressure is expected to respond to injection of fluid into the isolated interval during pumping and afterwards for various hydraulic diffusivities. We expect that for an isolated zone experiencing constant perturbation without the presence of natural fractures that pressure will increase linearly with time (Figure 2a and 2c). This is compared to the hypothetical scenario in which the presence of fractures will result in rolling over of the pressure curve since there is an increase in the volumetric capacity for pressure to diffuse into (Figure 2b and 2d). As the hydraulic diffusivity of pressure changes, we expect different responses in the pressure curves during perturbation (build up) (Figure 2e) and re-equilibration (Figure 2f).

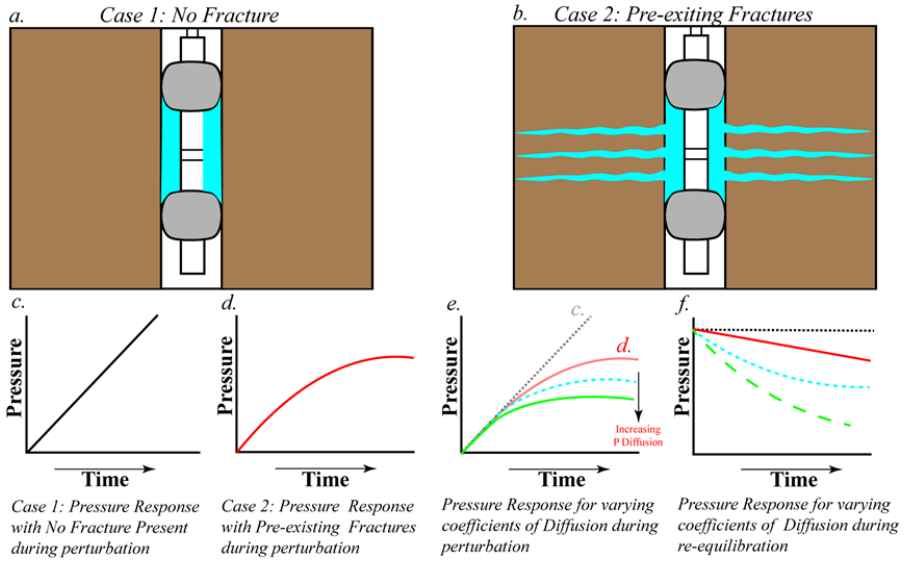

Figure 2. Schematic representation of the expected pressure behavior of injected fluid within an isolated zone for two scenarios. (a) No fracture presence and (b) presence of pre-existing fractures. Plots representing (c) a continuous linear pressure increase during perturbation for case 1, (d) roll over of pressure for case 2, (e) pressure buildup curves in response to varying hydraulic diffusivity and (f) pressure re-equilibration curves in response to varying hydraulic diffusivity.

4 RESULTS

4.1 Integrated Hydrogeologic Analysis

4.1.1 Neutron-Density Crossover and Sonic Porosity

We observed intervals of increased gas effect/neutron-density crossover from the difference in density and neutron porosity logs (Figure 3). The largest gas effects ais observed at around 7800 ft below the upper section of the Tribes hill Formation followed two other large signals - one above 8500 ft within the Little Falls Formation, the other above 9730 ft within the basement. Thicker groups of signals but with lower average values are observed within the lower section of the Tribes Hill Formation, the top (~8700 ft) and middle section (~9000 ft) of the Galway Formation, and from the bottom of the Galway Formation to through most of the Potsdam Group. The largest distribution and largest average values in sonic porosity extend from bottom of the Potsdam Formation to a section of basement. High signals spikes are also observed around 7800 ft below the upper section of the Tribes hill Formation, within the lower section of the

Little Falls Formation and its contact with the Galway Formation. Numerous lower signals are observed at sparse locations along the borehole.

4.1.2 Gas Chromatography

Numerous intervals with inflows of the inorganic gases hydrogen and helium are observed along the open borehole (Figure 3). Hydrogen gas concentrations show clear signals at several depth locations. These include signal spikes at around 7800 ft below the upper section of the Tribes hill Formation and ~9000 ft within the Galway formation. A larger distribution and concentration of signals in hydrogen is observed from the top of the basement contact (9430 ft) downward. Helium gas exhibits one significant spike in its signal along the open section at the very upper section of the Galway Formation. Sonic porosity exhibits numerous fluctuations in its signal along the borehole, however some sections show more prominent signals than others. A large spike in signal is observed on the upper section of the Tribes Hill Formation at ~7800 ft, followed by small, separated spikes with depth above 7900 ft. The next largest spike is observed below the Little Falls-Galway contact and has a much more grouped distribution of signals.

4.1.3 Fracture Interpretation

We observe non-uniform fracture distribution along the entire open section of the borehole (Figure 3). Fracture frequency is relatively low in the shallower section from about 7700 ft to around 8600 ft. This is followed by an increase in frequency within a narrow interval range at ~8700, then another decrease before a wider interval range of fracture frequencies toward the basement. The increased fracture frequencies are observed and can be grouped at several locations: the central region of the Little Falls Formation at ~8400 ft); the lower section of the Little Falls Formation; the upper section of the Galway Formation at ~8700 ft; the upper section of the Potsdam Group; and more than 100 ft from the basement contact downward. See companion paper by Fulcher et al., 2023 for detailed results on fracture analysis.

4.1.4 Hydrogeologic Airlift and Injection Test

Following the completion of all other wireline logging, testing, and sidewall coring operations, the mud was displaced out of the hole and replaced with ~1,092 bbls of clean water in addition to another 550 bbls of fresh water. Three hydrogeologic tests were conducted – one airlift test and two injection tests. For the airlift test, the well was shut in and a fluid level was established for ~12 hours before running a P-T (Pressure-Temperature) wireline survey to obtain static water level, indications of flow, and high-resolution pressure and temperature. A flowline was lowered to 1000 ft below the fluid level and whilst air was pumped, and water blown out of the hole through the flowline, pressure and temperature was recorded during and after the test. This was done prior to injection (i.e., pre-injection). The pre-injection measurements were obtained after shut-in of the well overnight. Based on observations of water level and P-T logs run during and after the airlift test primarily in spinner rotational velocities, the borehole did not appear to produce significant flow. Therefore, reinjection of the displaced water and pressurization with mud-pumps up to 1400 psig was then conducted to further determined potential permeable zones via inflow into formations. However, the re-injection spinner velocity logs also lacked any considerable information, suggesting that this procedure also did not appear to drive considerable flow into the formation Temperature Fluctuations

4.1.5 Temperature Fluctuations

A total of seven high resolution pressure-temperature logging runs were conducted at several stages throughout the hydrologic test, and changes to thermal the gradients were used to identify hydrologic signals related to permeability (see companion paper by Purwamaska and Fulton, 2023 for temperature interpretation and analyses). Residual temperatures of the seven temperature logs consist of observable short wavelength signals along the borehole (Figure 3). The residual temperatures were obtained using the pre-injection temperature profile as a reference geotherm based on a couple criteria, one of those pre-injection survey provides a temperature profile less perturbed by the hydrologic tests. The static temperature profile consists of a increasingly negative trend with depth that takes an obvious change in its long wavelength gradient profile after ~8700 ft, whilst the other temperature profiles consist of a fairly straight long wavelength gradient profile. When observing shorter wavelength changes in the temperature profiles, we notice several prominent signal fluctuations. Within the Tribe Hill Formation we notice a general decrease in residual temperatures which is strongly observed along the static test profile. Two strong changes in thermal gradients are observed in the Galway Formation: the first located at ~8700 ft which increases to the right; the second located above 9100 ft which decreases to the left. The strongest change in residual temperature for each recorded temperature log is observed immediately beneath the top of basement.

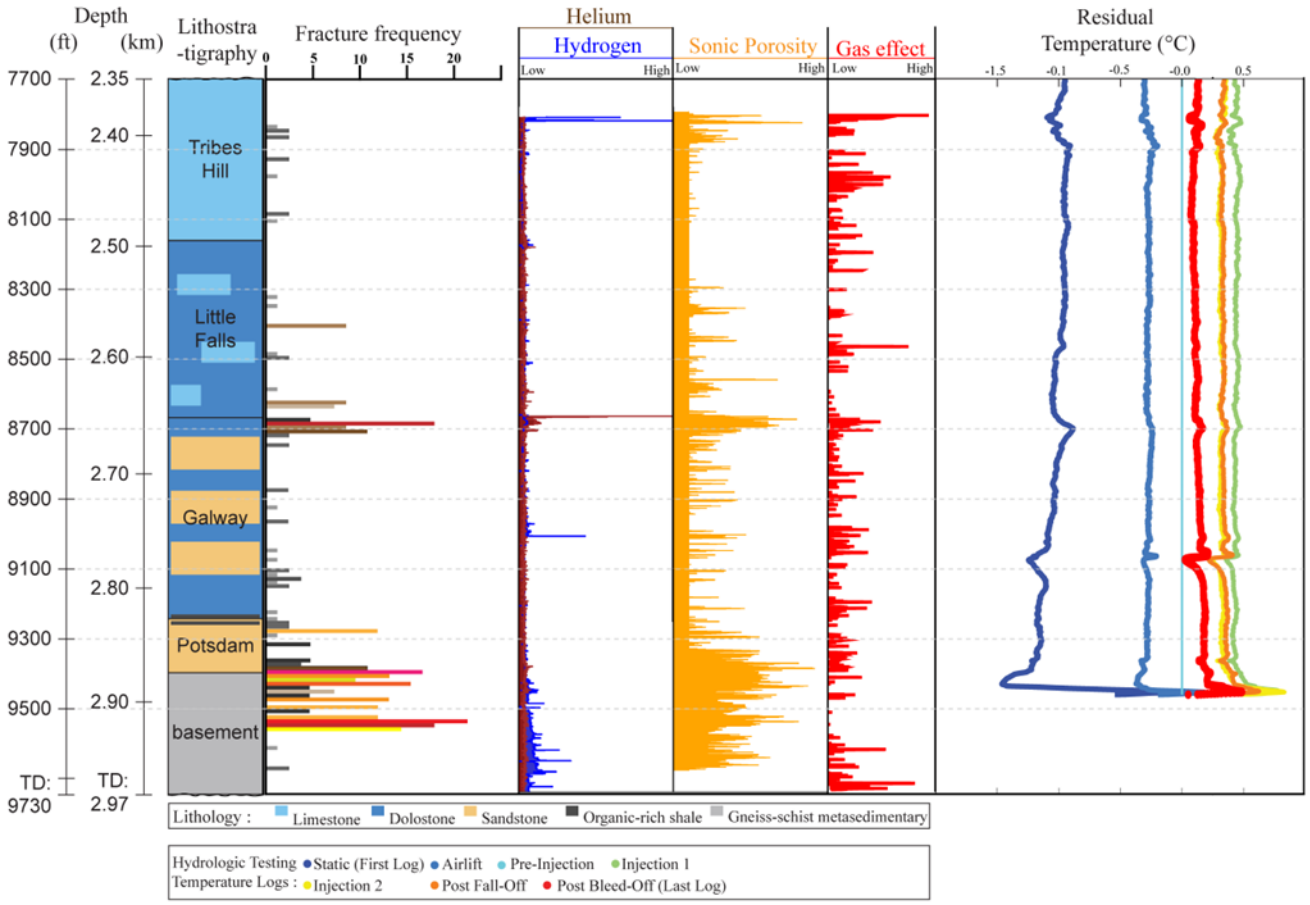

Figure 3. Combination of logs and interpretations to identify potential permeable zones. Schematic of lithologic column along the CUBO well: fracture frequency interpretation using a combination of acoustic and resistivity borehole imaging logs; inorganic gases, helium, and hydrogen obtain from a mass spectrometer; sonic porosity acquired from a 3D sonic scanner tool; gas/cross-over effect from neutron-density porosity logs and residual temperature for different types of tests during the airlift operation.

4.2 Pressure Diffusion Model

The result of the analytical pressure solution shows changes in the buildup and recovery curves for varying values of the hydraulic diffusivity (Figure 4). As expected, for extremely low values of the hydraulic diffusivity ($D = 1x10^{-6}$ and $1x10^{-5}$) pressure builds up linearly without any apparent change in the curve. During the re-equilibration period, pressure remains constant. Using an initial pressure of 0 MPa, the maximum pressure after 300 seconds reaches ~59 MPa for the lowest hydraulic diffusivity. Other models, not shown here, do indicate similar linear pressure build up and recovery with larger time (i.e. the maximum pressure increases as long as time also increases). As the value of hydraulic diffusivity increases, during perturbation the rate of pressure changes with time, beginning with a short linear rise before becoming more hyperbolic as the pressure reaches a lower maximum value with time (i.e. $D = 1x10^{-4}$ to $1x10^{-2}$). As for the re-equilibration period, the changes in gradient of the curve becomes more hyperbolic. For the lowest hydraulic diffusivity used in the model, the response of the pressure buildup and recovery is barely observed, theoretically indicating rapid diffusion of pressure.

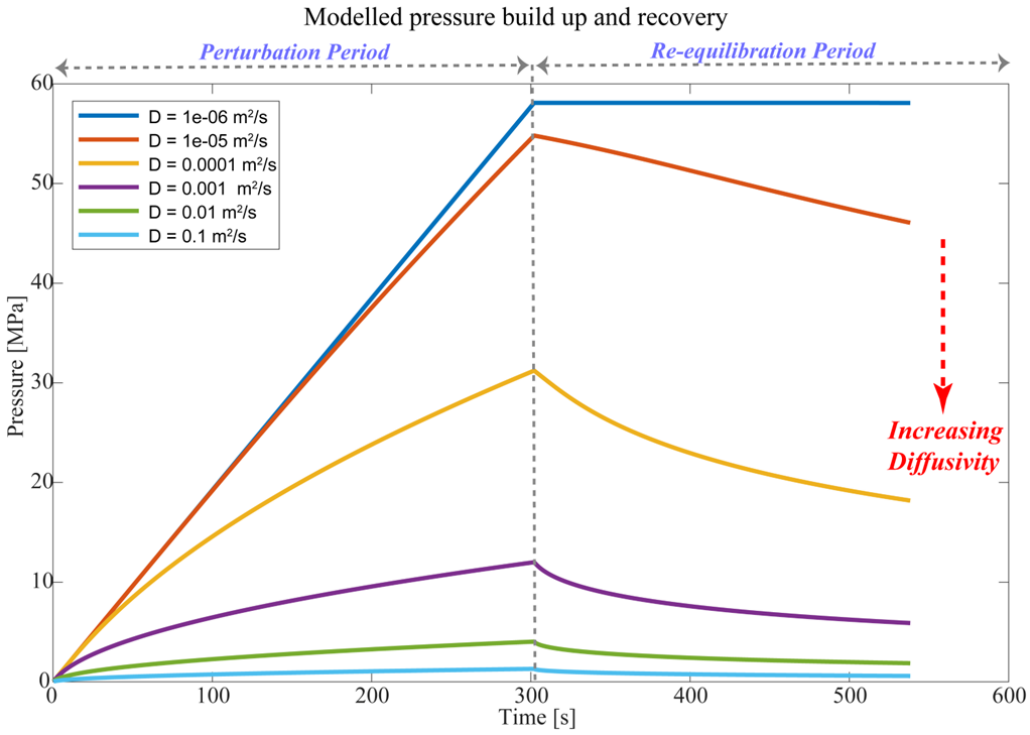

Figure 4. Modelled pressure build up and recovery for varying values of hydraulic diffusivity from 1 x 10^{-6} m^2/s to 1 x 10^{-1} m^2/s.

4.3 Dual-Packer Pressure Analysis

Five Dual-packer experiments were conducted at four depth locations (9360 ft, 8695 ft, 8685 ft, and 7885 ft) along the borehole. The experiments were taken in the following positions and order: experiment 1 at 9360ft within the lower Potsdam Formation; experiment 2 at 7885 ft within the Tribes Hill Formation; experiment 3 at 8685 ft, experiment 4 at 8695 ft; and experiment 5 at 8685 ft were all conducted within the upper Galway Formation. Pressurization was performed for each interval at experiments 1-4, whereas an additional experiment 5 was performed at interval depth 8685 ft. With the aid of the processed borehole imaging, the intervals which targeted in-situ fractures were experiments 3, 4 and 5, experiments 1 and 2 targeted zones without fractures. Each dual-packer test provided a suite of different measurements irrespective of pressure, including temperature, total pump-out volume, and total pump-out flow rate.

4.3.1 Hydraulic Diffusivity from Dual-Packer Test Analysis

We analyze pressure build up data during two dual-packer experiments, experiment four at 8695 feet and experiment 2 at 7885 feet (Figures 5 and 6). These mini-frac experiments show pressure roll-over during fluid injection prior to breakdown which represent pressure loss due to diffusion into the formation. We focus our analysis on pressure buildup curves during perturbation of the system (i.e. fluid injection).

For the 8695 ft depth dual packer injection experiment we observe several cycles of pressure build up coinciding with periods of active pumping (Figure 5). Three perturbation and re-equilibration cycles are observed (Cycles 1-3), whereas the fourth perturbation period leads to the break-down pressure of 75.28 Mpa. The initial pressures prior to perturbation are, 32.55, 44.46, 51.41 and 58.79 Mpa for Cycles 1-4 respectively. The initial pressures at the beginning of the re-equilibration periods are, 47.75, 60.25 and 72.8 Mpa for Cycles 1-3 respectively.

To model pressure diffusion, the following parameters were obtained from recorded measurements; the mass flow rate per volume (Q), determined from a conversion of the recorded average volumetric flow rate during each injection cycle, the compressibility of water used is 5 x 10^{-10} Pa^{-1}, and density of water used is 997 kg/m^3. The value of a ± x represents the radius of the borehole of 8.25 inches or 0.11 meters, hence the volume of the cylindrical 0.91 m packer interval is V = 0.0348 m^3. Therefore, we model the expected response of pressure at an observation located at a point along the borehole wall from its center. All parameters used in the models are listed in Table 1.

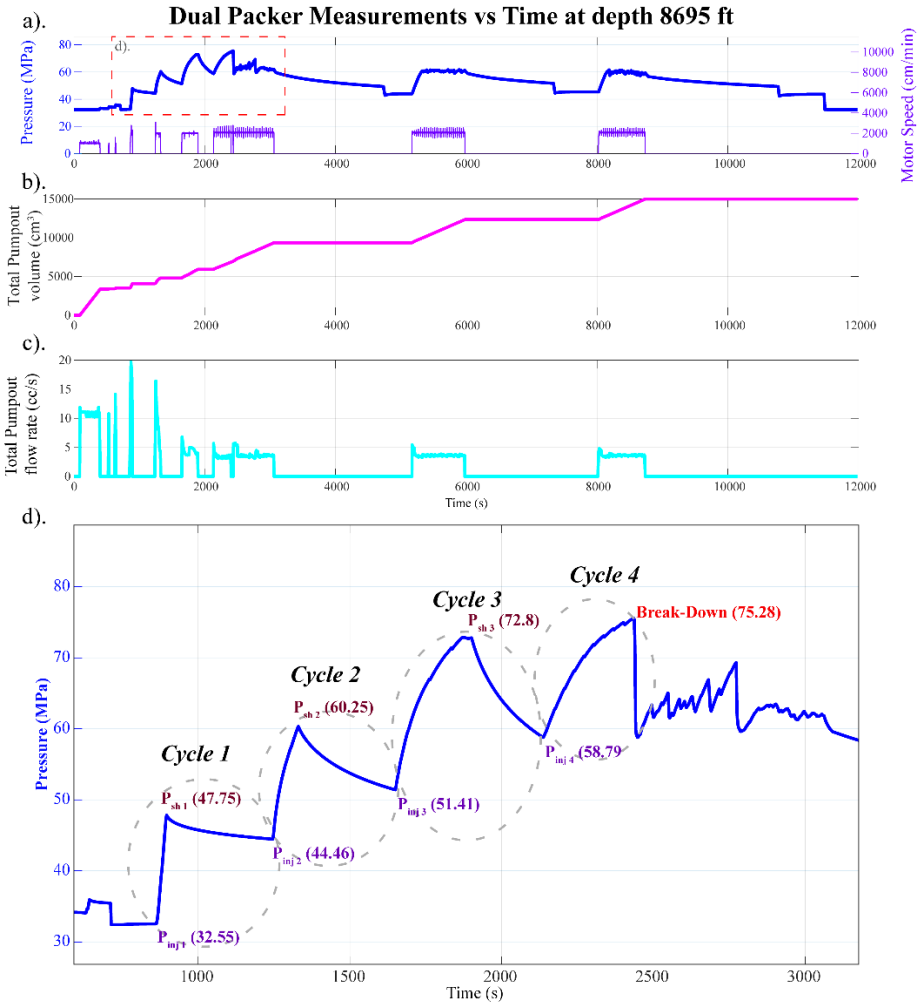

Figure 5. Measurements recorded during dual-packer experiment at depth 8695 ft. Measurements shown include (a) pressure and motor-speed, (b) total pump-out volume and (c) total pump-out flow rate. For the Zoom in figure (d) notice the pattern of pressure build-up and fall-off prior to breakdown pressure (Break-Down), may indicate intrinsic permeability due to pre-existing fractures. The 'flat' constant motor-speed values correspond to periods of injection. Four cycles of perturbation and re-equilibration of the system prior to the breakdown pressure are the focus for the applied model.

Table 1: Model parameters used for each buildup cycle at Depths 8695 ft and 7885 ft.

Cycle	Initial Pressure, P_i (MPa)	Volumetric flow rate, V_t (m^3/s)	Mass flow rate, m_t (kg/s)	Mass flow rate of fluid into isolated volume, Q (kg/m^3s)
Dual-Packer at Depth 8695 ft				
1	32.55	1.58 x 10-5	0.0158	0.45
2	44.46	8.55 x 10-6	0.0085	0.25
3	51.41	4.42 x 10-6	0.0044	0.12
4	58.79	3.34 x 10-6	0.0033	0.09
Dual-Packer at Depth 7885 ft				
1	29.64	1.71 x 10-5	0.0171	0.49
2	42.75	9.60 x 10-6	0.0096	0.29
3	55.59	3.70 x 10-6	0.0037	0.10
4	68.49	3.87 x 10-6	0.0039	0.11

Figure 7 shows the results of the models that best fit the observations of pressure with time, for the 4 cycles of buildup leading to the breakdown pressure. The hydraulic diffusivity values which best fit the models to the observed are 1.122 x 10^{-3}, 8.913 x 10^{-4}, 3.09 x 10^{-4} and 4.57 x 10^{-4} m^2/s, for Cycles 1-4 respectively. The average hydraulic diffusivity of the four values is 6.95 x 10^{-4} on the order of 10^{-4} m^2/s. Although the history of the model for Cycle 1 (Figure 7a) overestimates the prediction, the initial and final pressures closely coincide with the recorded pressure. Additionally, Cycle 2 (Figure 7b) and Cycle 4 (Figure 7d) consist of initial and final pressures that also match the observed as most of the modelled curve is well predicted, whereas for Cycle 3 (Figure 7c) the model overestimates the prediction toward the end. This may be due to the observed pressure curve flattening in the last ~50 seconds and is therefore not an ideal representation of the point at which the maximum pressure is reached. We also proceed to identify the relationship between the diffusion of pressure with subsequent perturbation and re-equilibration of fluid into the system during each cycle. It is shown that as the average pressure increases with each Cycle, the value of the hydraulic diffusivity decreases up to Cycle 3 before a jump at Cycle 4 shown in Figure 7e.

For experiment 2 at depth 7885 ft, Figure 6 shows the results of the models that best fit the observations for 4 cycles of buildup also. Three perturbation and re-equilibration cycles (Cycles 1-3) and a 4th perturbation period which increases to a break-down pressure of 80.13 Mpa (Figure 6). The initial pressures prior to perturbation are, 29.64, 42.74, 55.59 and 68.49 Mpa for Cycles 1-4 respectively. The initial pressures at the beginning of the re-equilibration periods are, 44.33, 57.45 and 70.83 MPa for ycles 1-3 respectively.

Figure 8 also shows the response of the modelled pressure with time for the cycles of buildup that lead to the breakdown pressure. The hydraulic diffusivity values which best fit the models to the observed are 1.99 x 10^{-3}, 1.20 x 10^{-3}, 1.23 x 10^{-4} and 4.37 x 10^{-4} m^2/s, for Cycles 1-4, respectively. The values provide an average hydraulic diffusivity of 9.39 x $10^{\wedge-4}$ m^2/s. Although the history of the model for Cycle 1 (Figure 8a) and Cycle 2 overestimates the prediction, the initial and final pressures match the recorded pressure. Cycles 2 (Figure 8b) and 3 (Figure 8d) consist of initial and final pressures that also closely match the observed as most of the modelled curved is well predicted. Upon comparing the average pressure during injection with corresponding hydraulic diffusivities we observed that as the average pressure increases with each cycle, the value of the hydraulic diffusivity decreases up to Cycle 3 before a jump at Cycle 4 shown (Figure 8f). The response is like the result of the dual-packer experiment at depth 8695 ft (See Figure 7f).

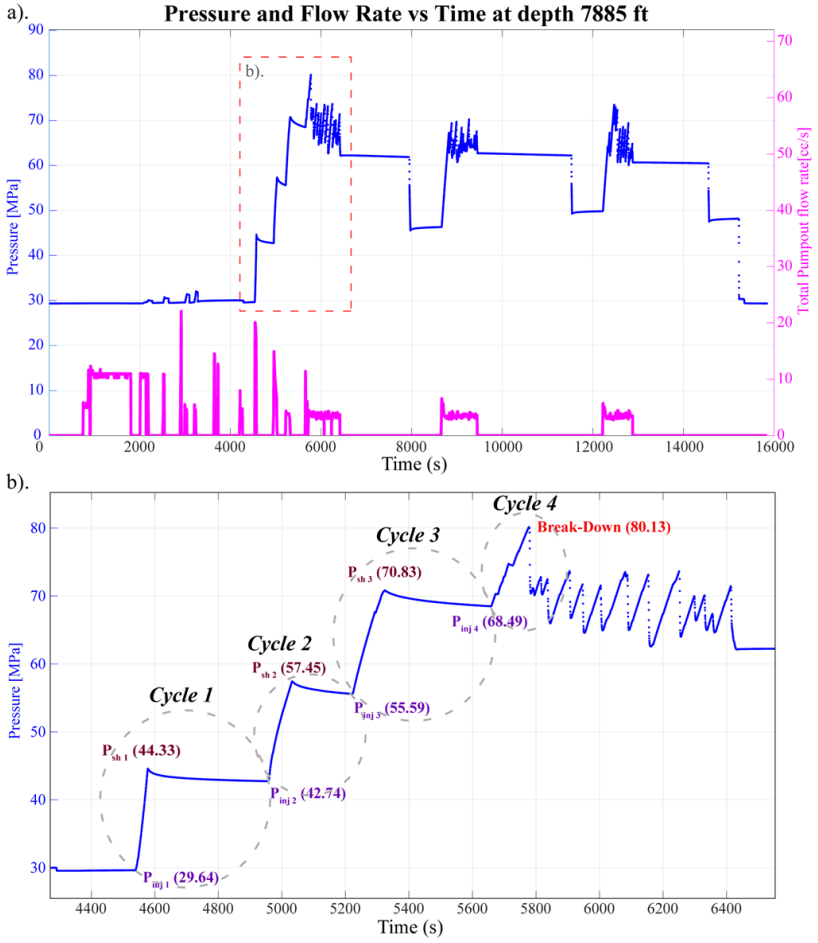

Figure 6. Measurements recorded during dual-packer experiment at depth 7885 ft. Measurements include (a) pressure and total pump-out flow rate. (b) In the Zoom-in of pressure notice the pattern of pressure build-up and fall-off prior to breakdown pressure (Break-Down) – may indicate intrinsic permeability due to pre-existing fractures. Four cycles of perturbation and re-equilibration of the system prior to the breakdown pressure are the focus for the applied model.

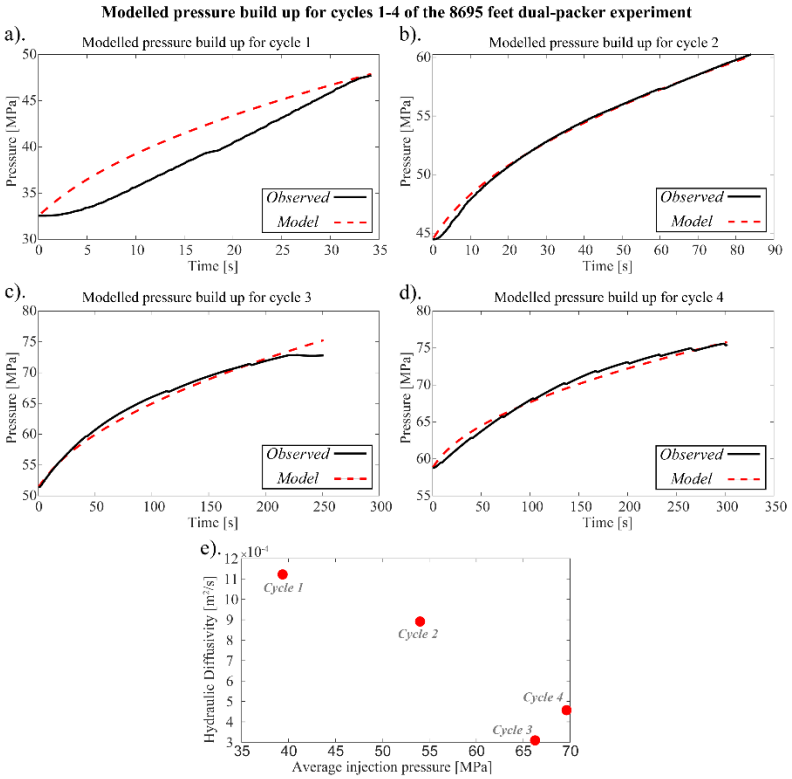

Figure 7. (a-d) Modelled pressure buildup for each observed cycle 1 through 4 prior to breakdown pressure at dual-packer 8695 ft. (e) Plot of the hydraulic diffusivities against the recorded average injection pressure of each cycle.

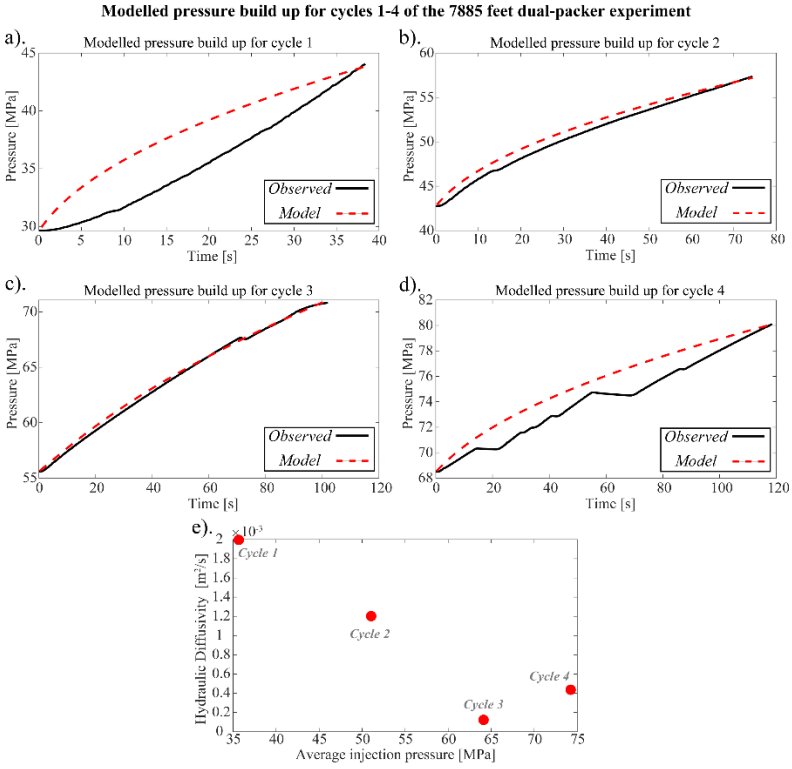

Figure 8. (a-d) Modelled pressure buildup for each observed cycle 1 through 4 prior to breakdown pressure at dual-packer 7885 ft. (e) Plot of the hydraulic diffusivities against the recorded average injection pressure of each cycle.

5 DISCUSSION

5.1 Integrated Analysis

The results of the hydrologic airlift test suggest an initial indication that the formations spanning the open section of the Ordovician-Pre-Cambrian strata are relatively low permeability. However, by integrating the results of fracture distribution and frequency; concentrations in inorganic helium and hydrogen; signals in neutron-density porosity cross-over and sonic porosity; and temperature fluctuations, we are able to locate and constrain zones with potential permeability. The first indication of permeability exists within the Upper Tribes hill Formation around 7800 ft (Figure 9). Here although the fracture frequency is relatively low, spikes in the signals of hydrogen, gas effect and sonic porosity align with a thermal anomaly observed in the residual temperatures (Purwamaska and Fulton, 2023). This may indicate high porosity but a poorly interconnected fracture framework. The second potentially permeable zone exists within the interval with the highest fluxes in inorganic helium and corresponds with a dense fracture frequency spanning dolomitized sandstone units of the Galway Formation between depths 8670 – 8710 ft. This zone also coincides with large sonic porosities, considerable gas effect and a clear thermal anomaly which deflects to the right. We suggest that the dominant type of porosity may be fractures and be considerably interconnected to permit fluid flow away from the borehole. Several hundred feet below, around 9100 ft, fracture frequency is relatively low, however correlation among the signal spikes in hydrogen, sonic porosity, gas effect and a thermal anomaly that deflects to the left suggest potential flow within this interval. Relatively low sonic porosity and hydrogen may be consistent with poor fracture interconnectivity and predominantly matrix porosity. The fourth interval which suggests permeability may exist, is found immediately beneath the Potsdam-basement contact within the largest distribution of high fracture frequencies. Additionally, this interval corresponds with the most significant thermal anomaly, is semi-correlated with rising hydrogen signals, is strongly correlated with the sonic porosity, but has a generally low gas effect. The correlations may indicate that fracture porosity may be the dominant porosity type within this zone. We identify each zone as Zone 1, Zone 2, Zone 3 and Zone 4 in the order discussed above (See Figure 9).

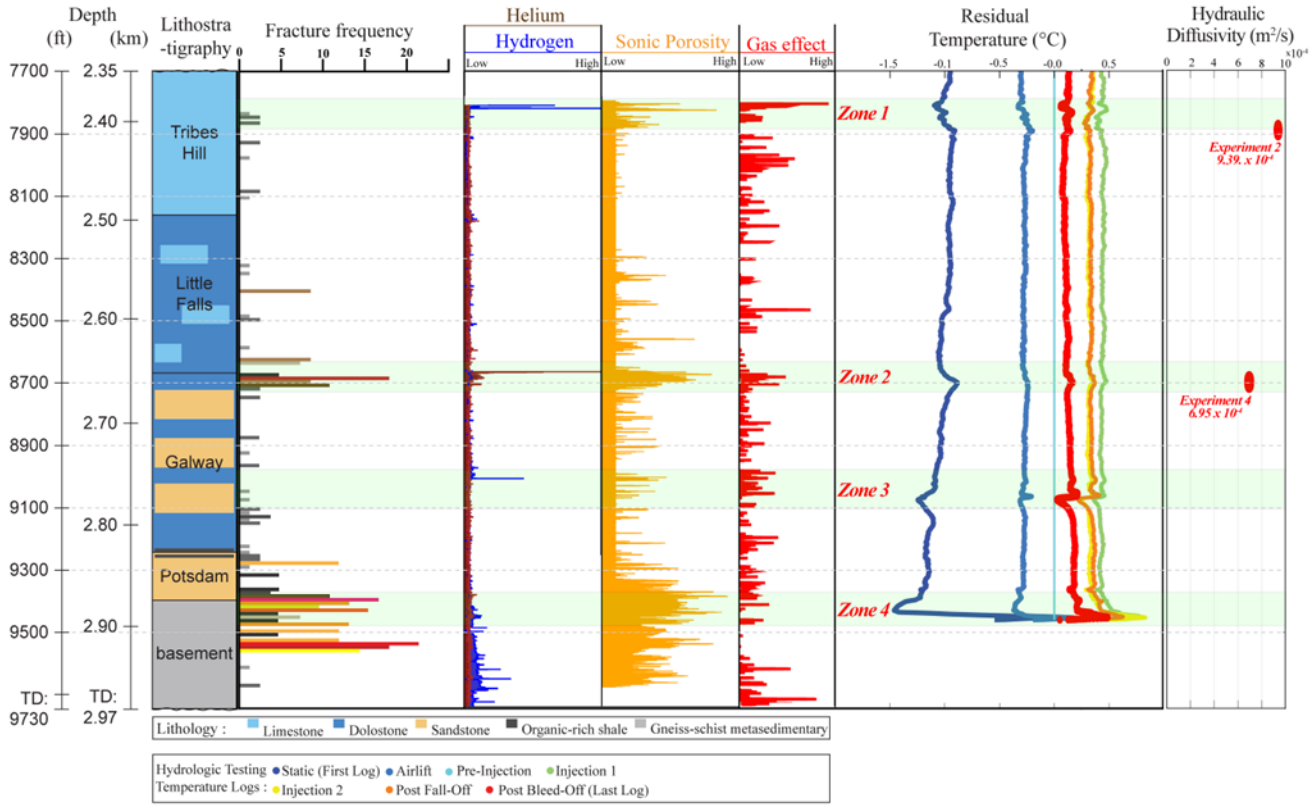

Figure 9. Combination of logs and interpretations to identify potential permeable zones. Four zones of potential permeability are identified based on the integrated analysis conducted. Schematic of lithologic column along the CUBO well: fracture frequency interpretation using a combination of acoustic and resistivity borehole imaging logs; inorganic gases, helium, and hydrogen obtain from a mass spectrometer; sonic porosity acquired from a 3D sonic scanner tool; gas effect/cross-over of neutron-density porosity logs; residual temperature for different types of tests during the airlift operation and hydraulic diffusivities determined from modelling pressure data of dual-packer experiments.

5.2 Quantitative Indicator of Permeability

We have determined quantitative hydrogeologic information from modelled pressure data, using a novel approach to the pressure diffusion equation. As aforementioned the initial solution by Lachenbruch (1986) and Fulton and Harris (2012), models the 1D temperature diffusion at a distance away from a thermogenic source – the source being along a faulted zone. Here, we aim to model the 1D pressure diffusion at the point at which the fluid enters natural fractures/pathways of a lithologic unit (i.e. along the borehole wall), during perturbation of the system. All interpretation and analyses are representative of the intrinsic permeability of rock, describing the hydrogeologic characteristics of natural pre-existing fractures prior to stimulation or inducing fractures. In the case where a system is completely contained, there is zero diffusion and only an increase in pressure as long as there is continuous perturbation of a fluid into the system. This rise in pressure follows a continuous linear trend (e.g. Figure 2c and Figure 4: D = $1x10^{-6}$). Positively increasing hydraulic diffusivities represent the ideal case in which pressure diffuses away as fluid escapes the contained volume simultaneously with perturbation (fluid injection). Larger hydraulic diffusivities are synonymous to increasing fracture frequency or larger fracture volume (i.e. length and aperture).

Although the 4 cycles for both Station 2 and Station 4 show an overall increase in pressure toward the breakdown pressure (See Figures 5d and 5b), the perturbation and re-equilibration curves for each cycle vary from one cycle to the next based on observation and the quantitative results obtained from the model. Two important observations from the quantitative results can be drawn: (1) the hydraulic diffusivities decrease from Cycles 1 to 3, before increasing at Cycle 4 and (2) the average of the hydraulic diffusivities is of the order 10^{-4} m^2/s. The first observation can explain the physical nature of pre-existing fractures re-opening with increasing fluid into the system during perturbation of the dual-packer experiment. For simplicity, we imagine the presence of a single horizontal or sub-horizontal fracture, extending laterally beyond either side of the borehole wall. Due to confining overburden stresses, the fracture may initially have a narrow aperture closing most of the fracture space and reducing the volume of fluid it can accommodate. However, we expect that to accommodate the increasing fluid volume away from the borehole, the pre-existing fracture reopens as pore fluid pressure exerts a force larger than the confining stresses. As the fracture re-opens in aperture and length across the lithologic unit, the permeability of the fracture should vary with each injection and re-equilibration cycle. We infer this process based on the different values of the hydraulic diffusivities used in the model to compare with the observations. However, the diffusivity values generally decrease with each cycle as more fluid is injected into the system, suggesting a decrease in permeability (Figure 7e and 8e). Though this may seem counterintuitive to the process described earlier, there is a possible explanation. It is likely that during the first perturbation and re-equilibration cycle (Cycle 1), the fracture accommodation space was large enough to allow for pressure to diffuse quickly. With the following second and third cycles, the accommodation space was less and filled to the point that the diffusion of pressure decreased subsequently. The rise of the hydraulic diffusivity at Cycle 4 may suggest the point of re-opening of a fracture and increasing the permeability. Since Cycle 4 represents the pressure build-up immediately before the breakdown pressure, the re-opening of an existing fracture may consequently then lead to creating a new opening of the propagating fracture.

Average values of hydraulic diffusivity have been shown to be on the order of 10^{-2} m^2/s in localized regions near active fault zones (i.e. the Wenchuan earthquake fault zone (Xue et al. 2013) and the San Andreas fault zone (Xue et al. 2016; Simon et al 2021)). Interestingly, those studies show uniform hydraulic diffusivities of around 10^{-2} m^2/s also, which reveals the response of the fracture networks to perturbation of the system. In this study, the average hydraulic diffusivities obtain at depths 8695 ft and 7885 ft are on the order of 10^{-4} m^2/s, two order of magnitudes lower than that in and near the mentioned active fault zones. In our study the perturbation is by a short-duration anthropogenic injection of fluid into a sedimentary layer within an intraplate setting as compared to an earthquake within an active region. The dual-packer experiment performed at depth interval 8695 ft targeted an interval with high frequency of fractures established by borehole imaging. Nevertheless, the fracture network may not be adequately dense or sufficiently well interconnected for pressure to diffuse easily into the formation. Not surprisingly, the localized fracture frequency and interconnectivity of fractures in an intraplate location with no known faults may not display similar hydraulic diffusivity as do fault zones. This plays an important role in identifying how localized fracture frequency and interconnectivity may vary in either setting.

6 CONCLUSION

The formations spanning the Ordovician-Pre-Cambrian strata beneath the ESH No.1 CUBO well may initially consist of relatively low permeability. However, there are indications of localized fracture permeability and connectivity based on the analyses on data from wireline logging and formation tests. This includes analyses done on fracture distribution and frequency; concentrations in inorganic helium and hydrogen; signals in neutron-density cross-over and sonic porosity; and temperature fluctuations. We identify 4 immediate zones based on correlations of a combination of all or several of the results. The four zones include: (a) Zone 1 around 7800 ft within the upper Tribes Hill Formation; (b) Zone 2 around 8695 ft at the top of the Galway Formation; (c) Zone 3 right above 9100 ft within the middle of interbedded dolomite and sandstone rocks of Galway Formation and (d) Zone 4 near 9430 ft, immediately beneath the Potsdam-basement contact. Dual packer experiments, primarily used for minifrac tests and stress analysis targeted 4 depth intervals (9360 ft, 8695 ft, 8685 ft, and 7885 ft), with a total of five experiments performed. We use a novel approach to model 1D pressure diffusion to obtain values of hydraulic diffusivity and hence quantitatively constrain intrinsic permeability of target intervals beneath the CUBO subsurface. Modelled pressure observations on the buildup curves from two of the five experiments, depths 8695 and 7885 ft, provide average hydraulic diffusivities of 6.95 x 10^{-4} and 9.39 x $10^{\wedge-4}$ m^2/s respectively. The hydraulic diffusivities provide further insight into the nature of permeability within or near two of the four zones. Future steps include determining hydraulic diffusivities from pressure data for the other dual-packer tests and performing analyses on the re-equilibration period of the pressure curves, while quantifying other hydrogeologic properties of potential reservoir targets along the borehole.

7 ACKNOWLEDGMENTS

This material presented in this paper is based upon work supported by the U.S. Department of Energy's Office of Energy Efficiency and Renewable Energy (EERE) under the Geothermal Technologies Office Award Number DE-EE0009255. The authors also acknowledge the support provided by Cornell University and the many contributions from other members of the Earth Source Heat project team.

Disclaimer: The views expressed in this paper do not necessarily represent the views of the U.S. Department of Energy or the United States Government

8 REFERENCES

Asquith, G. and Krygowski, D. (2004) Basic Well Log Analysis. AAPG Methods in Exploration Series, No. 16, (2004).

Beckers, K. F., Pauling, H., Kolker, A., Hawkins, A. J., Gustafson, J. O., Jordan, T. E., Fulton, P. M., & Tester, J. W. (n.d.). Geothermal Deep Direct-Use for Low-Carbon Heating: A Case Study at Cornell University, 9, (2021).

Carslaw, H. S., & Jaeger, J. C. Conduction of Heat in Solids, 282, (1959).

Earlougher, R. C. Advances in well test analysis (Vol. 5, pp. 165-166). New York: Henry L. Doherty Memorial Fund of AIME, (1977).

Fulton, P. M., & Harris, R. N. Thermal considerations in inferring frictional heating from vitrinite reflectance and implications for shallow coseismic slip within the Nankai Subduction Zone. Earth and Planetary Science Letters, 335–336, 206–215, (2012).

Fulcher, S.A., D. Pinilla, T.E. Jordan, & P.M. Fulton, Fracture Network Characterization and Permeability for Direct-Use Geothermal Energy – Cornell University Borehole Observatory ESH No. 1

Gustafson, J. O., Jordan, T. E., Brown, L. D., May, D., Horowitz, F., Beckers, K., & Tester, J. W. *Cornell University Earth Source Heat Project: Preliminary Assessment of Geologic Factors Affecting Reservoir Structure and Seismic Hazard Analysis*, 10, (2020).

Jordan, T., Fulton, P., Tester, J., Bruhn, D., Asanuma, H., Harms, U., Wang, C., Schmitt, D., Vardon, P. J., Hofmann, H., Pasquini, T., Smith, J., & the workshop participants. Borehole research in New York State can advance utilization of low-enthalpy geothermal energy, management of potential risks, and understanding of deep sedimentary and crystalline geologic systems. Sci. Dril. 28, 75–91 (2020). https://doi.org/10.5194/sd-28-75-2020

Lachenbruch, A.H. Simple models for the estimation and measurement of frictional heating by an earthquake. United States Geological Survey Open-File Report 86-508,13, (1986).

Malik, M., Jones, C. & Boratko, E. How Can Microfracturing Improve Reservoir Management? 16, (2016).

Matthews, C. S., & Russell, D. G. Pressure buildup and flow tests in wells (Vol. 1, p. 27). New York: Henry L. Doherty Memorial Fund of AIME, (1967).

Pinilla, D.G., P. M. Fulton, T.E. Jordan, Preliminary determination of in-situ stress orientation and magnitude at the Cornell University Borehole Observatory (CUBO) geothermal well, Ithaca NY.

Purwamaska, I. and P. M. Fulton, Preliminary Constraints on Thermal Conditions within the Cornell University Borehole Observatory (CUBO), Ithaca New York.

Simon, J. B., Fulton, P. M., & Xue, L. Hydrogeologic Property Estimation in Plate Boundary Observatory Boreholes Using Tidal Response Analysis. *Geofluids*, *2021*, 1–19, (2021). https://doi.org/10.1155/2021/6697021

Tester, J., Jordan, T., Beyers, S., Gustafson, O. & Smith, J. Earth Source Heat: A Cascaded Systems Approach to DDU of Geothermal Energy on the Cornell Campus. DOE-Cornell-8103-1, 1844600 https://www.osti.gov/servlets/purl/1844600/ , (2019). doi:10.2172/1844600.

Tester, J. W., Steve Beyers, J. Olaf Gustafson, Teresa E. Jordan, Jared D. Smith, J. A. Aswad, Koenraad F. Beckers et al. District geothermal heating using EGS technology to meet carbon neutrality goals: a case study of earth source heat for the Cornell University campus. In Proceedings of the World Geothermal Congress, vol 1, (2020).

Tester, J., Gustafson, J. O., Fulton, P., Jordan, T., Beckers, K., Beyers, S. Geothermal direct use for decarbonization - progress towards demonstrating Earth Source Heat at Cornell, 22, (2023).

Xue, L., Li, H.-B., Brodsky, E. E., Xu, Z.-Q., Kano, Y., Wang, H., Mori, J. J., Si, J.-L., Pei, J.-L., Zhang, W., Yang, G., Sun, Z.-M., & Huang, Y. Continuous Permeability Measurements Record Healing Inside the Wenchuan Earthquake Fault Zone. Science 340, 1555–1559, (2013). https://doi.org/10.1126/science.1237237

Xue, L., Brodsky, E. E., Erskine, J., Fulton, P. M., & Carter, R. A permeability and compliance contrast measured hydrogeologically on the San Andreas Fault. *Geochemistry, Geophysics, Geosystems*, *17*(3), 858–871, (2016). https://doi.org/10.1002/2015GC006167